Retrieving a common accumulation record from Greenland ice cores for the past 1800 years

K. K. Andersen, P. D. Ditlevsen, S. O. Rasmussen, H. B. Clausen, B. M. Vinther

and S. J. Johnsen

Ice and Climate, Niels Bohr Institute, University of Copenhagen, Copenhagen,

Denmark

K. K. Andersen, Ice and Climate, Niels Bohr Institute, University of Copenhagen, Denmark. (kka@gfy.ku.dk)

Abstract. In the accumulation zone of the Greenland ice sheet the annual accumulation rate may be determined through identification of the annual cycle in the isotopic climate signal and other parameters that exhibit seasonal variations. On an annual basis the accumulation rate in different Greenland ice cores is highly variable, and the degree of correlation between accumulation series from different ice cores is low. However, when using multi year averages of the different accumulation records the correlation increases significantly. A statistical model has been developed to estimate the common climate signal in the different accumulation records through optimization of the ratio between the variance of the common signal and of the residual. Using this model a common Greenland accumulation record with five years resolution for the past 1800 years has been extracted. The record establishes a climatic record which implies that very dry conditions during the 13th century together with dry and cold spells during the 14th century may have put extra strain on the Norse population in Greenland and have contributed to their extinction.

1. Introduction

The net precipitation rate in the accumulation zone of an ice sheet is recorded in the annual ice layer thickness profile which may be obtained from ice cores. However, due to local fluctuations and especially variations in the snow surface due to drift (sastrugies) the signal to noise variance ratio is rather poor, of the order 1–3, as established from comparisons of different shallow cores drilled close to one another [*Fisher et al.*, 1985]. The deep ice cores in Greenland are distributed mainly along the ice divide. As demonstrated by several authors these cores contain a common climatic signal over the large scale climatic changes during the last glacial period [e.g., *Johnsen et al.*, 2001]. In order to separate the common climatic information from local phenomena and noise for the shorter term variations during climatically stable periods it is however crucial to improve the signal to noise ratio. *Crüger et al.*, [2004] showed that it is problematic to assume a common signal in records from different sites on the Greenland ice sheet on short time scales, but we expect extreme features and long-term variations to be concurrent over large parts of Greenland.

2. The ice cores and ice flow

In this work we compare the annual ice layer thickness profiles from five Greenland ice cores. The cores were chosen to ensure relatively long accumulation records of annual resolution over a common time period. The cores used in this study are the DYE-3 [*Dansgaard et al.*, 1982], the Milcent [*Hammer et al.*, 1978], the Crete [*Hammer et al.*, 1980], the GRIP [*Johnsen et al.*, 1992] and the NorthGRIP (NGRIP) [*Johnsen et al.*, 2001; *NorthGRIP members*, 2004] ice cores. Details about the location, length and accumulation rates of these cores are given in Table 1.

The NGRIP, GRIP and Crete ice cores are all located very close to the ice divide, GRIP and Crete in the center of the Greenland ice sheet and NGRIP 324 kilometers NNW of the GRIP drill site. Milcent is in the central part of Greenland, but about 260 km west of the ice divide, whereas the DYE-3 drill site is located on the southern part of the ice sheet, about 30 km east of the ice divide. The ice cores used for this study are thus rather widely spaced, and all sites are subject to local meteorological conditions. Moreover the cores derive from both sides of the ice divide, which is known to influence the recorded signal [*Clausen et al.,* 1988; *Rogers et al.*, 2002] as the sites are affected by different air masses. Nevertheless it is expected that to a first approximation these ice cores share a common climate signal on an annual to decadal scale, which we here wish to extract. The accumulation rates were determined by identifying and counting annual layers as determined from the high resolution δ^{18}O and Electrical Conductivity Measurement (ECM) records. In the case of North GRIP these records were supported by Ion Chromatographic measurements at 5 cm resolution over the upper 350 m (Andersen et al., in preparation). The stratigraphy of the single cores has been cross-checked using known volcanic horizons and ECM as also described by Vinther et al. (in preparation). The dating uncertainty is estimated to be 1-2 years over the first millenium increasing to a few years at the end of the records used here.

In order to derive annual accumulation rates from the observed annual layer thicknesses, the data had to be corrected for densification and thinning of the ice layers due to ice flow. This was done by using a flow model [*Johnsen et al.*, 1992; *Johnsen et al.*, 1999] also accounting for the firnification at the top of the ice. In this way we obtained cross-dated chronological time series of annual accumulation rates over the latest two millenia, with relative dating errors being at most a few years. The ice flow in the DYE-3 region is complicated by upstream surface

undulations, and the obtained accumulation rate profile thus contains longer term variations of non-climatic origin [*Reeh*, 1989]. In order to remove these variations we have filtered the DYE-3 accumulation record with a Butterworth filter of order 3 with a cut-off frequency of 0.003 year^{-1}, eliminating the lowest frequency variations. The obtained accumulation records are shown as five year average values in Figure 1.

The most commonly used climatic parameter obtained from Greenland ice cores is the δ^{18}O record, which is a proxy for the temperature at the location of formation of the precipitation. However as indicated by model simulations [e.g. *Werner et al.*, 2000] the δ^{18}O signal is modulated by the amount of precipitation formed at a given time and temperature. The amount of precipitation is thus in some aspects a more direct climate signal than δ^{18}O. Across large-scale climatic changes, like the Dansgaard Oeschger events, there is a clear correlation between δ^{18}O and accumulation rates [*Dahl-Jensen*, 1993]. *Kapsner et al* [1995] and *Crüger et al* [2004] have however shown that both during the most recent Holocene and the transition out of the last glacial period atmospheric circulation had larger influence on accumulation than temperature. Figure 2 shows scatter plots of δ^{18}O versus the logarithm of the accumulation for the records used in this study. Although the correlation is rather weak it is thus expected that different information may be obtained from the two records, especially during relatively stable climate periods.

3. Statistical Distribution of Annual Layer Thicknesses

The time series of annual accumulation rates obtained after correction for flow and compression are shown in Figure 1. It may be seen that the variance of each record roughly scales with the mean value (note the different axis scaling). The statistical distribution of annual layer thicknesses from each of the drill sites is shown in Figure 3. The accumulation rates from especially Crete and Milcent take on discrete values, as these ice cores like the DYE-3 core were sampled with

a constant number of samples per year according to a predicted model time scale. The GRIP and NGRIP cores were cut in samples of constant size, and the discrete spectrum of values is changed into a continuous spectrum when correcting the annual layer thicknesses for the effect of layer thinning. The distributions are observed not to be symmetric around the mean. When plotted on a logarithmic accumulation axis the distributions become approximately symmetric, with a shape close to a normal distribution, as also observed by *Rasmussen et al.* [2005] for the accumulation record from the Early Holocene, Younger Dryas and Bølling sections of the NGRIP core. It may be expected that the accumulation rates follow Gamma distributions, as they are derived as the sum of positive independent precipitation events. Due to the discrete sampling rates and the limited number of annual layers in the records we can however not distinguish between this and a lognormal distribution. In the following we will for simplicity use the fact that the logarithm of the accumulation rates is approximately normally distributed.

4. The Noise Model

From the set of available accumulation series we want to estimate a common accumulation record signifying the variability in the mean regional precipitation over the past millenia. This signal is denoted $x(t)$. As pointed out by e.g. *Fisher et al.* [1985] the variance in the accumulation is ascribable to temporal, regional areal and local areal variability. We are here only interested in the common temporal variability. The local variability due to blowing snow and heterogenous snowfall is considerably diminished through temporal averaging over intervals of a few years. The regional areal variability may be ascribed to varying atmospheric circulation and storm track together with orography [*Ohmura and Reeh*, 1991; *Dethloff et al.*, 2002; *Crüger et al.*, 2004]

As a first approximation we can assume that the measured accumulation at site i, denoted $x_i(t)$, receives a contribution from the common signal $x(t)$ with some site specific scaling constant α_i.

In addition, $x_i(t)$ may contain regional variability, but it is here treated as noise such that the measured signal is given as,

$$x_i(t) = \alpha_i x(t) + \sigma_i \eta_i(t). \quad (1)$$

The residual $\eta_i(t)$ is assumed have zero mean and unit variance such that σ_i^2 is the variance of the residual term. Further we will assume that the residual terms at two different sites i and j are uncorrelated; $\langle \eta_i \eta_j \rangle = \delta_{ij}$, where $\langle \cdot \rangle$ represents the temporal mean. As shown above the measured accumulation rates x_i are lognormally distributed. The noise as defined here consists of two main contributions, the larger scale variability from site to site, which as a first estimate can be regarded as white noise, and the glaciological noise which is blue noise for annually resolved records [*Fisher et al.*, 1985]. The blue noise may be ascribed to blowing snow (sastrugies) and discrete measurements sampling but it can efficiently be reduced by temporal averaging, and the assumption that $\eta_i(t)$ can be regarded as white noise is thus reasonable if we use accumulation data averaged over intervals large enough to remove the blue noise characteristics of the glaciological noise.

Even though we do not know to which extent $x(t)$ is a stationary stochastic process we will treat it as such and define the (unknown) signal variance,

$$\sigma^2 = \langle x^2 \rangle - \langle x \rangle^2. \quad (2)$$

4.1. Temporal Averaging

After having corrected for layer thinning and snow compression the annual layer thickness is a measure of the accumulated precipitation including noise attributable to drifting snow.

If the climate signal is auto correlated over times longer than the sampling time the noise can be reduced by temporal averaging of the signal. By doing that we of course loose information on

the fluctuations of the climate signal on timescales faster than the averaging time. With only few noisy timeseries available some temporal averaging is however necessary in order to improve the signal to noise variance ratio. Consider two records $x_i(t)$ and $x_j(t)$ related according to (1). With $y_i \equiv x_i - \langle x_i \rangle$ and $y_j \equiv x_j - \langle x_j \rangle$ being the deviations from the average, the temporal average over any odd number m of points is,

$$\overline{y}_i(t) = \frac{1}{m} \sum_{k=-\mu}^{\mu} y_i(t+k),\ \mu = (m-1)/2. \tag{3}$$

The covariance between the series is then given by:

$$\langle \overline{y}_i \overline{y}_j \rangle = \frac{1}{m^2} \sum_{k=-\mu}^{\mu} \sum_{l=-\mu}^{\mu} \langle y_i(t+k) y_j(t+l) \rangle. \tag{4}$$

With the deviation from the climate signal being defined as $y = x - \langle x \rangle$ we have,

$$\begin{aligned} \langle y_i(t+k) y_j(t+l) \rangle &= \alpha_i \alpha_j \langle y(t+k) y(t+l) \rangle + \sigma_i^2 \delta_{ij} \delta_{kl} \\ &= \alpha_i \alpha_j c(k-l) + \sigma_i^2 \delta_{ij} \delta_{kl}, \end{aligned} \tag{5}$$

where we have introduced the autocovariance $c(\tau) = \langle y(t) y(t+\tau) \rangle$ for the climate signal. δ_{ij} is the Kronecker delta. By inserting this into (4) we obtain,

$$\begin{aligned} \langle \overline{y}_i \overline{y}_j \rangle &= \frac{1}{m} \alpha_i \alpha_j \left[c(0) + 2 \sum_{k=1}^{m-1} \frac{m-k}{m} c(k) + \frac{\sigma_i^2}{\alpha_i \alpha_j} \delta_{ij} \right] \\ &= \frac{1}{m} \alpha_i \alpha_j \left[I[c] + \frac{\sigma_i^2}{\alpha_i \alpha_j} \delta_{ij} \right], \end{aligned} \tag{6}$$

where $I[c] \equiv c(0) + 2 \sum_{k=1}^{m-1} c(k)(m-k)/m$. Finally we have the expression for the correlation coefficient,

$$\begin{aligned} C_{ij} &= \langle \overline{y}_i \overline{y}_j \rangle / \sqrt{\langle \overline{y}_i^2 \rangle \langle \overline{y}_j^2 \rangle} \\ &= \left[1 + \left(\frac{\sigma_i^2}{\alpha_i^2} + \frac{\sigma_j^2}{\alpha_j^2} \right) \frac{1}{I[c]} + \left(\frac{\sigma_i^2 \sigma_j^2}{\alpha_i^2 \alpha_j^2} \right) \frac{1}{I[c]^2} \right]^{-1/2}. \end{aligned} \tag{7}$$

If the climate signal is assumed to be a red noise signal with autocorrelation $c(t) = \sigma^2 \exp(-|t|/T)$, where T is the correlation time, then by approximating the sum with an integral we obtain,

$$I[c] = 2\sigma^2 T \left[1 + \frac{T}{m}(\exp(-m/T) - 1)\right]. \quad (8)$$

Figure 4 shows the correlation coefficients between all pairs of records used for this study, when averaging over an increasing numbers of years. Based on the findings in Section 3 the averages have been taken over the logarithm of the data. The maximum correlation of 0.72 is obtained between the GRIP and the Crete ice cores when averaging over more than 20 years. A correlation time of about 10 years may be anticipated, and a comparison with the result obtained from (7) using T=10 years agrees well with the ice core data for longer term averages (dashed curve in Figure 4). For short term averages the correlation coefficients between all pairs of records increase faster than the theoretical result of (7) in agreement with the blue noise spectrum observed by *Fisher et al.* [1985], while the curves follow the shape of the theoretical result for averaging lengths above 3-5 years. We thus conclude that the major part of the blue noise has been removed when averaging over 5 year intervals, and apply this averaging approach in the rest of this work, assuming that the residual term $\eta_i(t)$ can be regarded as white noise.

5. Determination of model parameters

With accumulation series from n ice cores we have to determine $2n + 1$ unknown parameters, namely (α_i, σ_i) for $i = 1, ..., n$ and σ. The overall magnitude of the climate signal is arbitrary, and we set $\langle x \rangle = 1$. The variance of the climate signal (2) then becomes $\sigma^2 = \langle x^2 \rangle - 1$. Equations for the signal scaling parameters α_i may be estimated from averaging (1) over the

whole length of the series,

$$\langle x_i \rangle = \alpha_i \langle x \rangle = \alpha_i. \tag{9}$$

Further equations can be derived from the covariance matrix. Assuming that the signals $x_i(t)$ are stationary processes the covariance c_{ij} between two signals may be calculated as

$$\begin{aligned} c_{ij} &= \langle x_i x_j \rangle = \langle (\alpha_i x + \sigma_i \eta_i)(\alpha_j x + \sigma_j \eta_j) \rangle \\ &= \alpha_i \alpha_j \langle x^2 \rangle + \sigma_i^2 \delta_{ij} \\ &= \alpha_i \alpha_j (\sigma^2 + 1) + \sigma_i^2 \delta_{ij}. \end{aligned} \tag{10}$$

The set of equations from (9) and (10) is overdetermined and is solved by finding the set of estimated parameters $\widetilde{\alpha}_i$, $\widetilde{\sigma}_i$, and $\widetilde{\sigma}$ that minimizes the total misfit M defined as

$$\begin{aligned} M &= \sum_{i=1}^{n} (\widetilde{\alpha}_i - \langle x_i \rangle)^2 \\ &+ \sum_{i=1}^{n} \sum_{j=i}^{n} \left(\widetilde{\alpha}_i \widetilde{\alpha}_j (\widetilde{\sigma}^2 + 1) + \widetilde{\sigma}_i^2 \delta_{ij} - \langle x_i x_j \rangle \right)^2. \end{aligned} \tag{11}$$

For the minimalization, the initial guesses were $\widetilde{\alpha}_i = \langle x_i \rangle, \widetilde{\sigma}_i = 0.8 \cdot std(x_i)$ and $\widetilde{\sigma}^2 = 0.002$, but the estimated parameter values are insensitive to the choice of initial guesses, as long as reasonable values are used.

6. The Optimal Climate Signal

We now want to use the results of the presented model to calculate an estimate $\tilde{x}(t)$ of the common climate signal $x(t)$ extracting maximum information on the common climate variability in the records. The method applied finds the linear combination of the individual records which optimizes the ratio between the variance of the common signal and the variance of the residual, as estimated from the model.

6.1. The accumulation reconstruction

Based on the model given in (1), equations (9) and (10) may be combined to give the expression for the variance of any of the measured series x_i

$$\langle x_i^2 \rangle - \langle x_i \rangle^2 = \alpha_i^2 \sigma^2 + \sigma_i^2. \tag{12}$$

With the presented model the ratio, F_i, between the total variance of a record and the variance of the residual is given as

$$F_i = \text{variance of record / variance of residual} = (\alpha_i \sigma / \sigma_i)^2 + 1. \tag{13}$$

The estimate $\tilde{x}(t)$ of the common climate signal will be constructed such that the model based ratio between the variance of the total signal and the residual is maximized. The linear combination is expressed as

$$\tilde{x}(t) = \sum_i \gamma_i x_i, \tag{14}$$

with the coefficients γ_i being determined such that $\tilde{x}(t)$ represents $x(t)$ as closely as possible. We can do this in two different ways which lead to the same result. Firstly the linear combination which maximizes $F_{\tilde{x}}$ may be found directly. Combining (1) and (14) one gets $\tilde{x}(t) = \sum_i (\gamma_i \alpha_i x(t) + \gamma_i \sigma_i \eta_i(t))$. The signal to residual variance ratio $F_{\tilde{x}}$ for any linear combination of x_i's may be expressed as

$$F_{\tilde{x}} = \frac{(\sum_i \gamma_i \alpha_i)^2 \sigma^2}{\sum_i (\gamma_i \sigma_i)^2} + 1, \tag{15}$$

from which we have,

$$\frac{\partial F_{\tilde{x}}}{\partial \gamma_k} = \frac{2\sigma^2 \sum_i \gamma_i \alpha_i}{(\sum_i (\gamma_i \sigma_i)^2)^2} \left[\alpha_k \sum_j (\gamma_j \sigma_j)^2 - \gamma_k \sigma_k^2 \sum_j \gamma_j \alpha_j \right]. \tag{16}$$

By redefining $\tilde{\gamma}_j = \gamma_j \sigma_j^2 / \alpha_j$ we get,

$$\frac{\partial F_{\tilde{x}}}{\partial \gamma_k} = 0 \Rightarrow \sum_j (\tilde{\gamma}_j - \tilde{\gamma}_k) (\frac{\alpha_j}{\sigma_j})^2 \tilde{\gamma}_j = 0, \tag{17}$$

with the solution $\tilde{\gamma}_j = \tilde{\gamma}$ for all j, where $\tilde{\gamma}$ is an arbitrary constant. From the definition above we thus get $\gamma_j = \alpha_j/\sigma_j^2$. As an alternative to maximizing the signal to residual variance ratio we can simply determine $\tilde{x}(t)$ by minimizing the root mean square error between a linear combination of the series $x_i(t)$ and (the unknown) $x(t)$. This results in the same linear combination as above. The estimated optimal climate record can thus be represented as,

$$\begin{aligned} \tilde{x}(t) &= \sum_i \left(\frac{\alpha_i}{\sigma_i^2}\right) x_i(t) \\ &= \sum_i \left(\left(\frac{\alpha_i}{\sigma_i}\right)^2 x(t) + \left(\frac{\alpha_i}{\sigma_i}\right) \eta_i(t) \right). \end{aligned} \tag{18}$$

The estimated model parameters determined for the five ice core records over the common time interval, A. D. 1177-1972 are given in Table 2. The values for α_i found by the minimalization procedure agree well with the accumulation rates given in Table 1, although those are averages over recent years, whereas the α_i's correspond to long term averages. As expected high σ_i's are found for the high accumulation sites. The model assumption that the residual signals are mutually uncorrelated was checked with the estimated series, and is largely confirmed. We find comparable modeled signal to residual variance ratios for all records cores investigated here, meaning that all cores have comparable influence on the common signal. DYE-3 has the lowest ratio, which probably reflects the fact the DYE-3 is located east of the ice divide and considerably further south than the other ice cores included in this study. The DYE-3 site receives a larger proportion of its precipitation from cyclonic activity associated with the Icelandic low than the other cores. Moreover as mentioned earlier the DYE-3 accumulation record had to be corrected for ice flow at the site. When comparing the signal to residual ratios in this study with the signal to noise ratio estimates by *Fisher et al.* [1985] their values, especially for DYE-3, are considerably higher than what is found here (note that the definition of their ratios correspond to equation (13)minus 1). *Fisher et al.* [1985] in their study investigated the local signal to

noise variance ratio by comparing the noise in a number of ice cores drilled close to another, whereas we here aim at the common signal over Greenland, considering everything else as the residual. The definition of noise in the two studies is thus inherently different and can not readily be compared.

6.2. Sensitivity of the reconstruction

The stratigraphically dated records used in this study are of different lengths. The Crete and Milcent ice cores are intermediate length ice cores of about 400 m, and the length of the records presented is determined by the length of the cores. The DYE-3, GRIP and NGRIP ice cores are all deep ice cores reaching back through the last glacial period. The length of the annual accumulation records presented here is determined by the length of the stratigraphically dated uppermost part of the ice cores. The length of each stratigraphy is limited by the initial accumulation rate at the site determining the isotopic diffusion, together with the sampling resolution and the location of the brittle zone in the cores. The accumulation at the DYE-3 drilling site is high enough to preserve annual cycles in the isotopic signal throughout most of the Holocene. *Hammer et al.* [1986] used this fact to count annual layers continuously back to 5.9 ka BP and in sequences to about 8 ka BP. Vinther et al. (in preparation) have refined the isotopic measurements and present an improved Greenland stratigraphy for the past 8.2 ka. This together with the work of *Rasmussen et al.* [2005] comprises the new "Greenland Ice Core Chronology 2005" (GICC05) throughout the Holocene period, combining and cross-dating the best available measurements from the NGRIP, GRIP and DYE-3 records. In the work presented, the DYE-3 and GRIP stratigraphies have only been used over the period common with the NGRIP accumulation record.

From the five cores we have calculated three estimates of the common accumulation curve as shown in Figure 5. The three curves are constructed by using the three, four, and five longest records over their common period, respectively. The three resulting curves show convincing agreement over their common periods, and all major minima and maxima recur in all curves. We will thus in the following treat the longest record, based on NGRIP, GRIP and DYE-3 as a common accumulation rate reconstruction.

When estimating the parameters for the optimal climate curve, the original accumulation data are first averaged over discrete five year bins. These bins can of course be constructed in five different ways, and Figure 6 illustrates the variability associated with the choice of bins. Although differences are obvious, choosing a different set of bins does not significantly change the location of prominent maxima and minima.

6.3. The accumulation and the isotopic climate records

The resulting accumulation curve is displayed together with the corresponding stacked $\delta^{18}O$ signal in Figure 6. As expected the two curves show only few similarities when compared with five year resolution over the past 1800 years. A few commonalities may however be noted. Accumulation rates as well as $\delta^{18}O$ values show a decreasing trend over the 8th and 9th centuries followed by a steeper increase around A. D. 900 and another decrease over the following centuries. The decreasing trend in accumulation rate after A. D. 1800 is one of the few features in Figure 5 which actually depend on which cores are involved in the reconstruction. A weak decrease is found in NGRIP, but+ a stronger decrease is mainly seen for DYE-3 (Figure 1), with low values around A. D. 1950 and just before A. D. 1970. We do not consider this a regional Greenland signal, but a local South Greenland signal, probably connected to atmospheric circulation changes. The slight increase in $\delta^{18}O$ over the past centuries is again strongest in DYE-

3, but is also found for NGRIP. In NGRIP it is however followed by low values during the 1980's and early 1990's which are not included in the common period investigated here. On top of these longer term variations the latest centuries of the common accumulation and $\delta^{18}O$ curves are characterized by concordant faster variations. Synchronous minima are found around 1836, 1873, 1883 and 1910 to 1920. Large volcanic eruptions are known to have climatic influence and in Greenland also to influence the $\delta^{18}O$ values. Most of these common minima in fact may be connected to volcanic eruptions. The minima in 1836 coincide with the eruption of Coseguina, Nicaragua with a Volcanic Explocivity Index (VEI) of 5 in late 1835. The minima in the early 1880s are most probably related to the 1883 Krakatoa eruption. The minima around 1865 can however not immediately be connected to any volcanic eruptions.

Synchronous sharp decreases in the presented common accumulation and $\delta^{18}O$ records may thus often be related to larger volcanic events. On the other hand smaller eruptions with smaller effect on climate may result in decreases in accumulation rate and $\delta^{18}O$ for all of the investigated cores within one or two years, even though this does not emerge from the combined five year records displayed here. When looking at the earliest part of the record very low $\delta^{18}O$ values are found around A. D. 530, probably connected to a strong volcanic horizon in A. D. 529. Despite the very low $\delta^{18}O$ values a corresponding drop in accumulation is not found, although it coincides with a longer period of relatively low accumulation rates. A second strong minimum in $\delta^{18}O$ is found around A. D. 680, but the apparently corresponding minimum in accumulation is in fact not synchronous, it only occurs 20 years later, around A. D. 700.

6.4. Climatic implications of the common accumulation record

Focusing on the common accumulation record in Figure 6 some very interesting features may be noted. Several occurrences of very dry spells are found during the periods A. D. 450, 700,

around A. D. 1000 (especially 1040 and 1080), and again in the 13th century with a broad minimum just around A. D. 1200. Somewhat weaker minima are found in A. D. 1380, 1640 to 1700, and in the beginning of the 20th century. Around year A. D. 450 and 700 only one 5 year period shows exceptionally low accumulation, whereas during the 11th and 13th centuries the periods with low accumulation are part of more persistent features. The early part of the Greenland accumulation record presented here agrees well with findings from the Igaliku Fjord in Southern Greenland. *Jensen et al.* [2004] using sediment cores from southern Greenland reported cold and moist climate condition between A. D. 500 and 700. The period between A. D. 800 and 1250 is reported to have been very variable with increased wind stress. The 11th century climate curve presented here is characterized by high variability and several periods with low accumulation. The 13th century also contains several periods with very low accumulation, but moreover the 13th century is characterized by conditions generally drier than normal, and a complete absence of 5 year intervals with high accumulation. The presented accumulation and temperature proxy record shows that climate conditions in this period were harsh and put extra strain on the population, as already noted by [*Dansgaard et al.*, 1975]. The 13th century shows three deep accumulation minima, beginning with the deep minimum at 1200 A. D.. Each of these represents five to ten year intervals with a mean precipitation about 10 % lower than the long term mean. The mid-14th to early 15th century is the time when the Norse population disappeared in Greenland, and the Western Settlement is believed to have lain waste around A. D. 1360 [*Lynnerup et al.*, 2004]. The 14th century is seen to have been cold with spells of very dry conditions, most markedly around 1380 where both the accumulation and isotope record have a distinct minimum. Unusually dry periods may thus very well have contributed to the demise of the Norse population. The sustainability of pasture and livestock was marginal

even under 'normal conditions' [*McGovern*, 2000], and the Norse in the Eastern Settlement designed irrigation constructions directing water from high lakes into their fields. This laborious undertaking strongly indicates that precipitation and water supply was indeed critical for farming and grassing fields. The deep minimum in the record around 1200 A. D. also precedes a period where a shift towards a more marine diet (fish and seal) is observed [*Arneborg et al.*, 1999]. It is commonly assumed that the reason for the decline of the Norse settlements was the change to a colder climate in the little ice age, however, this happened on a much longer time scale than the spells of very low precipitation. This means that we must expect that it was easier for Norse farmers to adapt to the change in temperature, and the drought could have initiated the Norse abandoning farming and their ultimate disappearance.

A sharp increase in accumulation occurs around year 1400, with the highest values recorded over the whole period. This sudden increase in accumulation coincides with the abrupt increase in sea-salt concentration in the GISP2 ice core [*Kreutz et al.*, 1997] interpreted as increased meridional atmospheric circulation intensity at the onset of the little ice age. In our reconstructed accumulation record, besides a shorter dry interval around 1480, both the variability and the accumulation rates remained high until the second half of the 17th century. About 10 % lower than average accumulation rates are found for 1690 to 1710, followed by increased accumulation rates and decreased variability. The little ice age period may thus only be seen as a shallow relative minimum during the period from 1600 to 1700 in the common accumulation record presented here.

6.5. Spectral analysis

Spectral analysis has been carried out on the estimated accumulation record. Very little long-term variation is contained in the record, the lowest frequency significant peak corresponds to

a wavelength of 56 years. Other significant peaks are found for 22.6, 16.6, 12.7, 11.8 and 10.4 years, which points to a solar influence on the accumulation record. The peaks in the 10-13 years interval are marginally resolved when we use 5 year averaged data, but the same analysis has been carried out with 3 and 4 year averages, resulting in the same spectral peaks.

7. Other reconstructions of a common accumulation record

In order to test the robustness of our results we also calculated a common accumulation record using several other methods. Besides the model presented in this paper we computed the simple stack of the available accumulation series, the "α-stacked" series and the first principal component derived using the five accumulation records averaged over 5 years for the period A. D. 1177 to A. D. 1972.

7.1. Stacking the records

As an obvious choice the optimal record has been compared to a simple stack

$$x_s(t) = \frac{1}{n} \sum_i x_i(t) \tag{19}$$

of the original records. A probably more appropriate method is what we here call the "α-stack",

$$x_{as}(t) = \frac{1}{n} \sum_i \frac{x_i(t)}{\alpha_i} \tag{20}$$

where all records are scaled down by their mean accumulation before stacking. As discussed here and in Fisher et al. [1985] the variance of individual accumulation records is approximately proportional to the average annual accumulation rate, which makes this approach very reasonable.

7.2. Principal component analysis

The third comparison was made performing a Principal Component Analysis (PCA) on the accumulation data. The PCA analysis was performed on the 5 year logarithmically averaged

accumulation data in order to avoid the blue noise. In analogy with the α-stack each series was hereafter divided by its mean value, whereafter all series were centered around zero for the analysis, i. e. $z_i(t) = x(t) + (\sigma_i/\alpha_i)\eta_i(t) - 1$

Table 3 displays the weights on the first three EOFs. All ice core records have about equal positive weight on the first EOF, except for NGRIP where the weight is somewhat lower. DYE-3 however has a very strong weight on the second EOF, and with opposite sign to all the other cores. The second principal component (not shown) thus strongly reflects the accumulation signal from DYE-3, and the correlation between the two is 0.77. This again reflects that the DYE-3 site is subject to local atmospheric processes and that the record contains considerable local climatic information, which is consistent with the relatively low signal to residual variance ratio found by the model for DYE-3.

The first principal component is displayed in Figure 8 together with the records obtained by the accumulation, the stacking and the α-stacking of the five ice core records averaged over 5 year bins for the period A. D. 1170 to A. D.1972 . The four curves are very similar, the main differences are seen in the amplitude of the minima and maxima.

7.3. Signal to residual variance ratio of the different signals

Based on the model 1 presented here signal to residual variance ratios may be calculated for the different reconstruction approaches. The signal to residual variance ratio of the optimal record is $F_{\bar{x}} = \sum_i (\alpha_i/\sigma_i)^2\sigma^2 + 1$, where the signal to residual variance ratios of the individual records are $F_i = (\alpha_i/\sigma_i)^2\sigma^2 + 1$. Stacking the n records, $x_s(t) = 1/n \sum_i x_i(t)$, gives the signal to residual variance ratio, $F_s = \sum_i \alpha_i^2 / \sum_i \sigma_i^2\sigma^2 + 1$, and the α-stack results in a signal to residual variance ratio $F_{as} = N^2\sigma^2 / \sum_i (\sigma_i/\alpha_i)^2 + 1$.

As the principal components are linear combinations of the original data series the model signal to residual variance ratio may be calculated in the same manner as described in section 6.1. The series used for the PCA are $z_i(t) = x(t) + (\sigma_i/\alpha_i)\eta_i(t) - 1$, and the principal components are linear combinations $z_{pc} = \sum_i e_i z_i$ where e_i is the loading for z_i. This results in $F_{pc} = (\sum_i e_i)^2\sigma^2 / \sum_i(\sigma_i e_i/\alpha_i)^2 + 1$

The estimated signal to residual variance ratios for the obtained reconstructions are given in Table 4. α-stacking results in somewhat higher values than the principal component analysis, and the simple stacking gives a significantly lower value than the others.

8. Summary and conclusion

A method has been presented to extract a common Greenland accumulation record of five year resolution over the past 1800 years. Annual accumulation records contain blue noise attributable to depositional effects, and this noise may be diminished by temporal averaging over a few years. We here used accumulation rate records from five Greenland ice cores which have been very thoroughly cross-dated. The common accumulation record was extracted by optimizing the ratio between the variance of the common signal and of the residual signal in all ice core records. The obtained signal has been compared to the stacked five year averaged $\delta^{18}O$ record from the same cores, and very little agreement is found, the two records thus contain different climatic information. Several episodic events with concordant lower than average accumulation rates and $\delta^{18}O$ values may be related to known larger volcanic eruptions. The obtained record of the common accumulation rate is quite robust with regard to the number of ice cores included in the reconstruction, and it compares well to reconstructions based on other methods, the main

difference being in the amplitude of variations and the calculated signal to residual variance ratio.

The 1800 years accumulation record shows longer term variations in accumulation rate over Greenland with especially the 13th and 14th centuries being persistently drier that normal, and with several very dry periods and a lack of unusually wet periods. This may very well have put additional strain on the Norse population in Greenland, and thus have contributed to their extinction.

Although accumulation rates over Greenland are highly dependent on local and regional features it has been demonstrated that a common Greenland accumulation record may be extracted from very precisely dated records. The noise in the obtained climate signal has been minimized by temporal averaging, and the local contribution was separated by the optimization procedure. The obtained record should thus be a more valuable input to hemispheric and global scale climate reconstructions than records from single ice cores.

9. Data access

The reconstructed accumulation record is available from http://icecores.dk.

Acknowledgments. Discussions with David Fisher and Jette Arneborg are greatly appreciated. KKA was supported by the Danish National Science Foundation of Denmark and the Carlsberg Foundation.

References

Arneborg, J., J. Heinemeier, N. Lynnerup, H. L. Nielsen, N. Rud and A. E. Sveinbjörnsdottir (1999), Change of Diet of the Greenland Vikings determined form stable carbon isotope analysis and 14 C dating of their bones., *Radiocarbon 41(2),* 157–168.

Clausen, H. B., N. Gundestrup, S. J. Johnsen, R. Bindschadler, and J. Zwally (1988), Glaciological investigations in the Crête-area, Central Greenland. A search for a new deep-drilling site, *Annals of Glaciology, 10,* 10–15.

Crüger, T., H. Fischer, and H. von Storch, What do accumulation records of single ice cores in Greenland represent? (2004), *J. Geophys. Res.*, , *109*, D21110, doi:10.1029/2004JD005014.

Dahl-Jensen, D., S. J. Johnsen, C. U. Hammer, H. B. Clausen and J. Jouzel (1993), Past Accumulation rates derived from observed annual layers in the GRIP ice core from Summit, Central Greenland, *Ice in the climate system, NATO ASI Series*, vol. 12, edited by W. R. Peltier, pp. 517–532, Springer-Verlag Berlin Heidelberg.

Dahl-Jensen, D., N. S. Gundestrup, H. Miller, O. Watanabe, S. J. Johnsen, J. P. Steffensen, H. B. Clausen, A. Svensson and L. B. Larsen (2002), The NorthGRIP deep drilling programme, *Annals of Glaciology, 35*, 1–4.

Dansgaard, W., S. J. Johnsen, N. Reeh, N. Gundestrup, H. B. Clausen, C. U. Hammer (1975), Climatic Changes, Norsemen and modern man, *Nature 255*, 24–28.

Dansgaard, W., H. B. Clausen, N. Gundestrup, C. U. Hammer, S. J. Johnsen, P. M. Kristinsdottir and N. Reeh (1982), A New Greenland Deep Ice Core, *Science, 218*, 1273–1277.

Dethloff, K., M. Schwager, J. H. Christensen, S. Kiilsholm, A. Rinke, W. Dorn, F. Jung-Rothenhäusler, H. Fischer, S. Kipfstuhl, and H. Miller (2002), Recent Greenland accumulation estimated from regional climate model simulations and ice core analysis, *Journal of Climate,*

15(19), 2821–2832.

Fisher, D. A., N. Reeh and H. B. Clausen (1985), Stratigraphic noise in time series derived from ice cores, *Annals of Glaciology, 7*, 76–83.

Hammer, C. U. et al., Dating of Greenland ice cores by flow models, isotopes, volcanic debris, and continental dust (1978), *Journal of Glaciology 20,* 3–26.

Hammer, C. U., H. B. Clausen and W. Dansgaard (1980), Greenland ice sheet evidence of post-glacial volcanism and its climatic impact, *Nature, 288*, 230–235.

Hammer, C. U., H. B. Clausen, and H. Tauber (1986), Ice-core dating of the Pleistocene/Holocene boundary applied to a calibration of the ^{14}C time scale, *Radiocarbon, 28(2A)*, 284–291.

Jensen, K. G., A. Kuijpers, N. Koç and J. Heinemeier (2004), Diatom evidense of hydrographic changes and ice conditions in Igaliku Fjord, South Greenland, during the past 1500 years, *the Holocene 14*, 2, 152–164.

Johnsen, S. J., H. B. Clausen, J. Jouzel, J. Schwander, A. E. Sveinbjörnsdottir, and J. White (1999), Stable Isotope Records from Greenland Deep Ice Cores: The Climate Signal and the Role of Diffusion, in *Ice Physics and the Natural Environment, NATO ASI Series*, Vol. 156., edited by J. S. Wettlaufer et al, pp. 89–107, Springer Verlag.

Johnsen, S. J. and W. Dansgaard (1992), On flow model dating of stable isotope records from Greenland ice cores. in *The last Deglaciation: Absolute and Radiocarbon Chronologies, NATO ASI Series*, Vol. 12, edited by E. Bard and W. S. Broecker, pp. 13–24, Springer-Verlag Berlin Heidelberg.

Johnsen, S. J., H. B. Clausen, W. Dansgaard, K. Fuhrer, N. Gundestrup, C. U. Hammer, P. Iversen, J. Jouzel, B. Stauffer and J. P. Steffensen (1992), Irregular glacial interstadials recorded in a new Greenland ice core, *Nature, 359*, 311–313.

Johnsen, S. J., D. Dahl-Jensen, N. Gundestrup, J. P. Steffensen, H. B. Clausen, H. Miller, V. Masson-Delmotte, A. E. Sveinbjörnsdottir, and J. White (2001), Oxygen isotope and palaeotemperature records from six Greenland ice-core stations: Camp Century, Dye-3, GRIP, GISP2, Renland and NorthGRIP, *Journal of Quaternary Science, 16(4)*, 299–307.

Kapsner, W. R., R. B. Alley, C. A. Shuman, S. Anandakrishnan, and P. M. Grootes (1995), Dominant influence of atmospheric circulation on snow accumulation in Greenland over the past 18,000 years, *Nature, 373(6509)*, 52–54.

Kreutz, K. J., P. A. Mayewski, L. D. Meeker, M. S. Twickler, S. I. Whitlow, and I. I. Pittalwala (1997), Bipolar changes in atmospheric circulation during the Little Ice Age, *Science, 277*, 1294–1296.

Lynnerup, N., S. Nørby, (2004), The Greenland Norse: bones, graves, computers, and DNA, *Polar Record 40 (213)*, 107–111.

McGovern, T. H. (2000), The Demise of Norse Greenland in: W.W. Fitzhugh, and E.I. Ward: *Vikings the North Atlantic Saga.* Smithsonian Press, Washington and London, 327–339.

North Greenland Ice-Core Project (NorthGRIP) Members (2004), High resolution Climate Record of the Northern Hemisphere reaching into the last Glacial Interglacial Period, *Nature*, 431(7005), 147–151.

Ohmura, A., and N. Reeh, New precipitation and accumulation maps for Greenland (1991), *Journal of Glaciology, 37*, 125, 140-148.

Rasmussen, S. O., K. K. Andersen, A. M. Svensson, J. P. Steffensen, B. M. Vinther, H. B. Clausen, M.-L. S. Andersen, S. J. Johnsen, L. B. Larsen, M. Bigler, R. Röthlisberger, H. Fischer, K. Goto-Azuma, M. E. Hansson, and U. Ruth (2005), A new Greenland ice core chronology for the last glacial termination, *J. Geophys. Res.*, , in review.

Reeh, N. (1989), Dating by ice flow modeling: A useful tool or an exercise in applied mathematics?, in *Dahlem Konference: The Environmental Record in Glaciers and Ice Sheets,* edited by U. Oeschger and C. C. Langway Jr.,

John Wiley, New York.

Rogers, J. C., J. F. Bolzan, V. A. Pohjola (2002), Atmospheric circulation vari- ability associated with shallow-core seasonal isotopic extremes near Summit, Greenland, *J. Geophys. Res., D10,* 11,205-–11,219.

Vinther, B. M., Johnsen, S. J., Andersen, K. K., Clausen, H. B., and A. W. Hansen (2003), NAO signal recorded in stable isotopes of the Greenland ice cores, *Geophys. Res. Lett., 30,* No. 7, 1387, DOI:10.1029/2002GL016193.

Werner, M., U. Mikolajewicz, M. Heimann, G. Hoffmann (2000), Borehole versus isotope temperatures in Greenland: Seasonality does matter, Geophysical Research Letters, 27, 723–726.

Figure Captions

Figure 1: The flow corrected accumulation series used in this work. The data data are shown as 5 year average values.

Figure 2: Scatter plots of the 5 years averaged logarithm of the accumulation rate and δ^{18}O for the whole length of the four longest series. The black lines indicate the best linear fits to the data with slopes of 1.71, 1.83, 2.1 and 0.44. The very low dependence for DYE-3 may be due to problems in the correction for ice flow. Correlations between ln(accumulation) and δ^{18}O are 0.17, 0.20 , 0.31 and 0.09, which are all significant at the 95% level.

Figure 3: The distribution of annual accumulation rates. The discrete values of the accumulation rates are obvious, especially for the shorter Crete and Milcent cores, but also for NGRIP, where a very high frequency is found around 19 cm. Distributions are plotted both on a linear and a logarithmic scale, and the distributions are seen to be more symmetric on the logarithmic scale. The distribution curves from the longest records, DYE-3 and GRIP, have been fitted to normal distributions on the logarithmic scale.

Figure 4: Correlation between the logarithm of the accumulation time series from the different ice cores. The correlation improves with averaging length as the noise decreases. The dashed line displays the correlation coefficient as calculated when using the estimated parameters for GRIP and Crete in (7) and assuming a correlation time of 10 years. The curve was re-scaled for the comparison. The increase in correlation between the cores observed for averaging lengths below 5 years grows faster than for the theoretical result. This is probably due to the removal of blue noise, and an averaging time of 5 years was used in this work.

Figure 5: The optimal accumulation records based on three, four, and five cores, depending on the length of the records. The different reconstructions bear a large resemblance over the common interval A. D. 1178-1973.

Figure 6: The optimal accumulation record over the period 188 A. D. to 1972 A. D. The curve has been constructed from the 5 year averaged accumulation records from DYE-3, GRIP and NGRIP. For every year the curve shown here is the average value of the results obtained when using five different averaging bins. The highest and lowest values found for every year are indicated by the grey envelope in order to illustrate the model variability associated with the different binning. The corresponding curve of the stacked $\delta^{18}O$ records from the three sites is displayed below. The apparent increase in $\delta^{18}O$ over the most recent decades derives mostly from the DYE-3 core.

Figure 7: Spectral analysis of the longest reconstruction based on the NGRIP, GRIP and DYE-3 records. Spectral peaks indicated on the plot are significant above the 95 % level in an MTM analysis. The same major spectral peaks arise when using data averaged over 3 and 4 year intervals.

Figure 8: The resulting accumulation profiles over the period A. D. 1177-1972 using different methods as described in Sections 6 and 7. The curves have been moved relatively to each other in the vertical direction. The parameters and the signal to residual ratios calculated for the different climate series are given in Tables 2 and 4.

Ice Core	Position	Acc. rate [m(i.e.)/yr]	Year drilled	Oldest year counted
NGRIP	75.10 °N 42.32 °W	0.19	1996	188 A. D.
GRIP	72.58 °N 37.64 °W	0.23	1993	
Crete	71.12 °N 37.32 °W	0.30	1974	554 A. D.
Milcent	70.30 °N 44.55 °W	0.53	1973	1177 A. D.
DYE-3	65.18 °N 43.83 °W	0.56	1979	

Table 1. Location, annual accumulation rate (in meters of ice equivalent) and time span covered by the stratigraphically dated ice cores used for this study. Apart from NGRIP these are the same cores that were used by *Vinther et al.* [2003]. The stratigraphic dating of the GRIP and DYE-3 cores has recently been extended over most of the Holocene (B. Vinther, in preparation), but we here use them over their common period with NGRIP, back to A. D. 188.

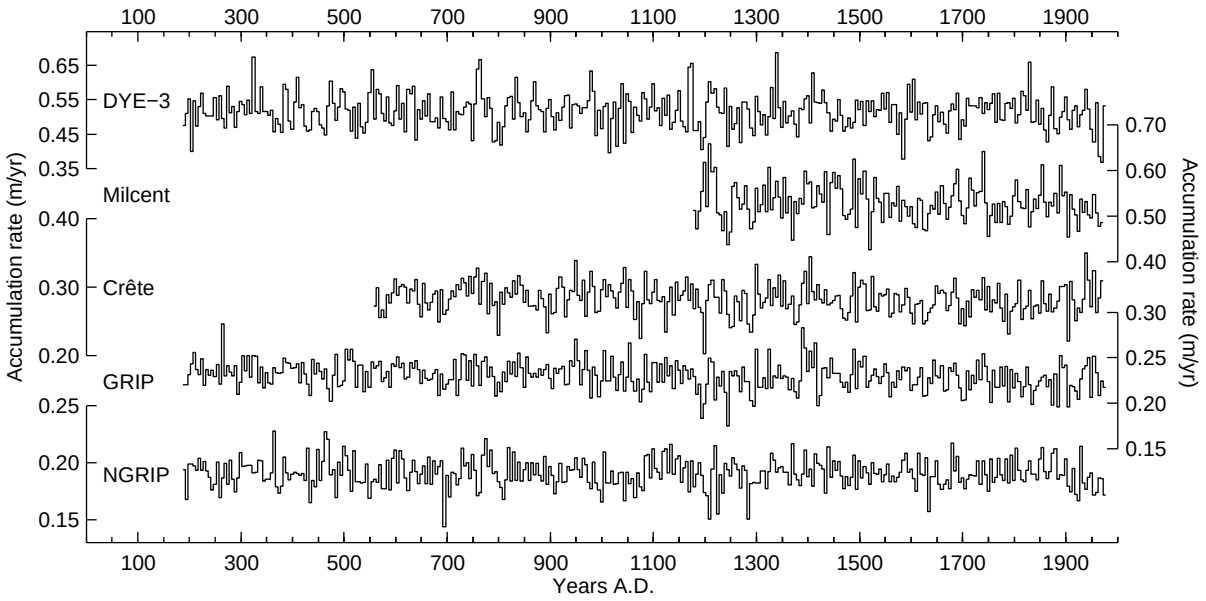

Figure 1. The flow corrected accumulation series used in this work. The data data are shown as 5 year average values.

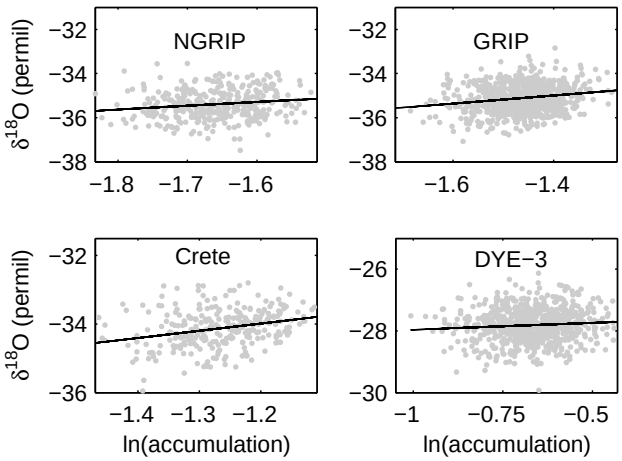

Figure 2. Scatter plots of the 5 years averaged logarithm of the accumulation rate and δ^{18}O for the whole length of the four longest series. The black lines indicate the best linear fits to the data with slopes of 1.71, 1.83, 2.1 and 0.44. The very low dependence for DYE-3 may be due to problems in the correction for ice flow. Correlations between ln(accumulation) and δ^{18}O are 0.17, 0.20 , 0.31 and 0.09, which are all significant at the 95% level.

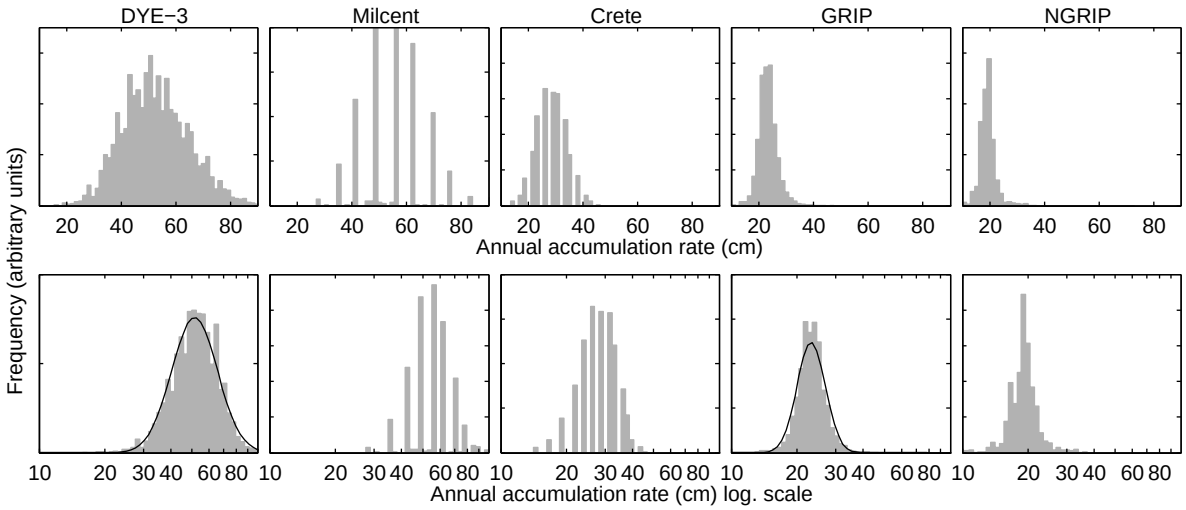

Figure 3. The distribution of annual accumulation rates. The discrete values of the accumulation rates are obvious, especially for the shorter Crete and Milcent cores, but also for NGRIP, where a very high frequency is found around 19 cm. Distributions are plotted both on a linear and a logarithmic scale, and the distributions are seen to be more symmetric on the logarithmic scale. The distribution curves from the longest records, DYE-3 and GRIP, have been fitted to normal distributions on the logarithmic scale.

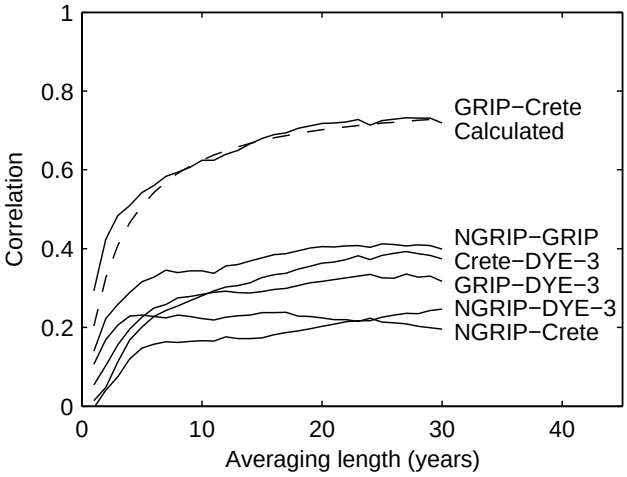

Figure 4. Correlation between the logarithm of the accumulation time series from the different ice cores. The correlation improves with averaging length as the noise decreases. The dashed line displays the correlation coefficient as calculated when using the estimated parameters for GRIP and Crete in (7) and assuming a correlation time of 10 years. The curve was re-scaled for the comparison. The increase in correlation between the cores observed for averaging lengths below 5 years grows faster than for the theoretical result. This is probably due to the removal of blue noise, and an averaging time of 5 years was used in this work.

Ice core	α_i	σ_i	γ_i	F_i
NGRIP	0.19	1.05e-2	0.382	1.50
GRIP	0.23	1.29e-2	0.300	1.47
Crete	0.28	1.90e-2	0.170	1.33
Milcent	0.53	3.55e-2	9.27e-2	1.34
DYE-3	0.51	4.59e-2	5.37e-2	1.19

Table 2. The values of α_i, σ_i, γ_i and the model signal to residual variance ratio, F_i, for the five records, when averaging over five year intervals for the period A. D. 1177-1972.

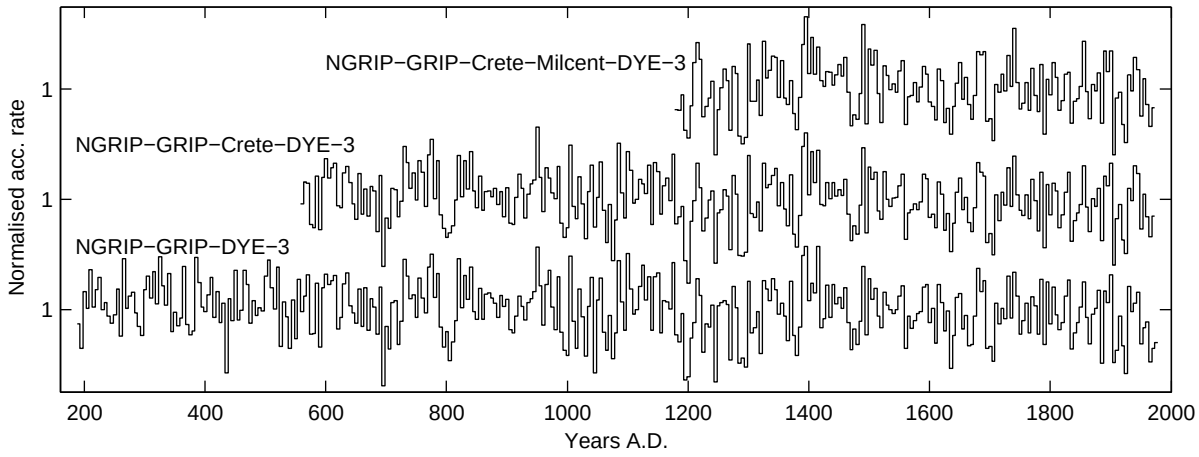

Figure 5. The optimal accumulation records based on three, four, and five cores, depending on the length of the records. The different reconstructions bear a large resemblance over the common interval A. D. 1178-1973.

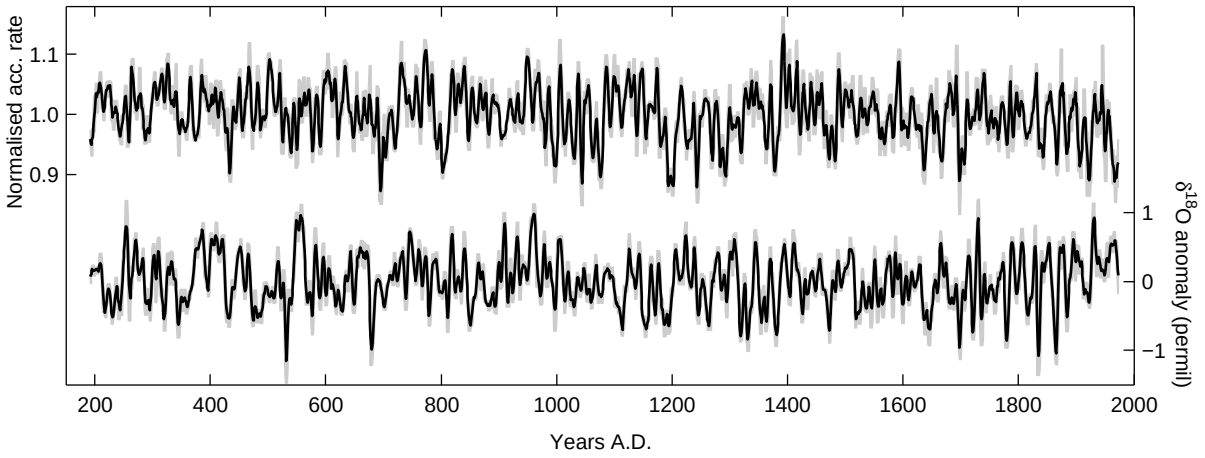

Figure 6. The optimal accumulation record over the period 188 A. D. to 1972 A. D. The curve has been constructed from the 5 year averaged accumulation records from DYE-3, GRIP and NGRIP. For every year the curve shown here is the average value of the results obtained when using five different averaging bins. The highest and lowest values found for every year are indicated by the grey envelope in order to illustrate the model variability associated with the different binning. The corresponding curve of the stacked $\delta^{18}O$ records from the three sites is displayed below. The apparent increase in $\delta^{18}O$ over the most recent decades derives mostly from the DYE-3 core.

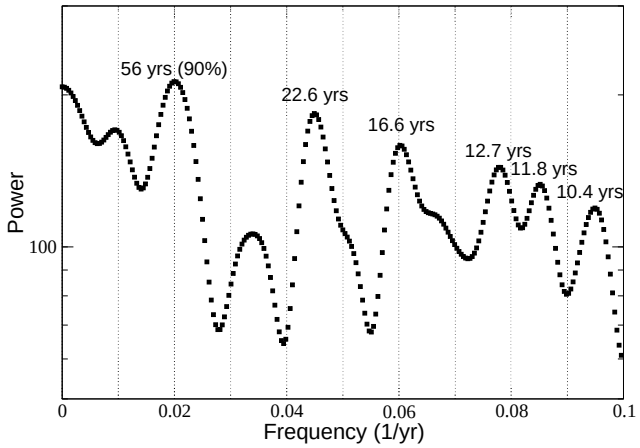

Figure 7. Spectral analysis of the longest reconstruction based on the NGRIP, GRIP and DYE-3 records. Spectral peaks indicated on the plot are significant above the 95 % level in an MTM analysis. The same major spectral peaks arise when using data averaged over 3 and 4 year intervals.

Ice core	EOF1	EOF2	EOF3
NGRIP	0.17	0.019	-0.60
GRIP	0.46	0.28	0.25
DYE-3	0.52	-0.85	0.010
Crete	0.54	0.32	0.45
Milcent	0.43	0.32	-0.61
Variance (%)	43.6	24.7	13.1

Table 3. The first three EOFs based on the five accumulation series averaged over 5 years for the period A. D. 1177-1972. On average over the five possible sets of bins the carried variances are 44.7%, 24.8% and 13.0%.

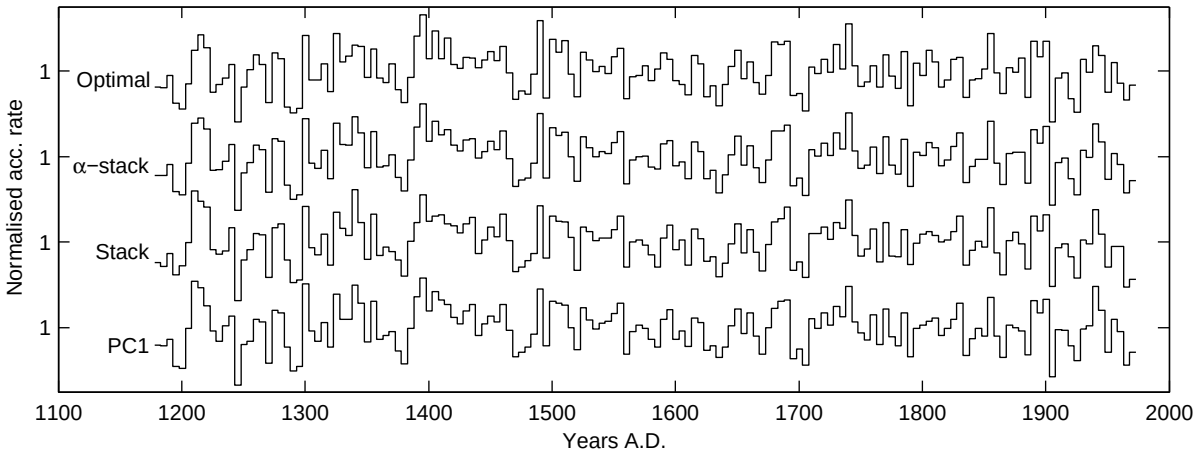

Figure 8. The resulting accumulation profiles over the period A. D. 1177-1972 using different methods as described in Sections 6 and 7. The curves have been moved relatively to each other in the vertical direction. The parameters and the signal to residual ratios calculated for the different climate series are given in Tables 2 and 4.

Ice core	Model	α-Stack	Stack	PC1
S/R	3.2	2.8	2.2	2. 5
S/R ratio:	$\frac{Model}{\alpha - Stack}$	$\frac{Model}{Stack}$	$\frac{Model}{PC1}$	
	1.1-1.2	1.3-1.6	1.2-1.4	

Table 4. Signal to residual variance ratios for the different calculated records. The values are averages of the five values obtained with different five year bin configurations. The ratios between the signal to residual variance ratios for the different methods are given below.